

Analysis of MINIE2013 Explosion Air-Blast Data

October 14, 2016

Report to the National Nuclear Security Administration,
Defense Nuclear Non-Proliferation Research &
Development, Nuclear Forensics, F-2016 Venture

Julie Schnurr¹, Arthur Rodgers, Keehoon Kim, Sean Ford and Abelardo Ramirez

Geophysical Monitoring Program

Lawrence Livermore National Laboratory

Livermore CA 94551

¹ Also at University of Hawaii, Manoa, HI 96822



Disclaimer

This document was prepared as an account of work sponsored by an agency of the United States government. Neither the United States government nor Lawrence Livermore National Security, LLC, nor any of their employees makes any warranty, expressed or implied, or assumes any legal liability or responsibility for the accuracy, completeness, or usefulness of any information, apparatus, product, or process disclosed, or represents that its use would not infringe privately owned rights. Reference herein to any specific commercial product, process, or service by trade name, trademark, manufacturer, or otherwise does not necessarily constitute or imply its endorsement, recommendation, or favoring by the United States government or Lawrence Livermore National Security, LLC. The views and opinions of authors expressed herein do not necessarily state or reflect those of the United States government or Lawrence Livermore National Security, LLC, and shall not be used for advertising or product endorsement purposes.

Lawrence Livermore National Laboratory is operated by Lawrence Livermore National Security, LLC, for the U.S. Department of Energy, National Nuclear Security Administration under Contract DE-AC52-07NA27344.

Summary

We report analysis of air-blast overpressure measurements from the MINIE2013 explosive experiments. The MINIE2013 experiment involved a series of nearly 70 near-surface (height-ofburst, HOB, ranging from -1 to +4 m) low-yield (W=2-20 kg TNT equivalent) chemical highexplosives tests that were recorded at local distances (230 m – 28.5 km). Many of the W and HOB combinations were repeated, allowing for quantification of the variability in air-blast features and corresponding yield estimates. We measured canonical signal features (peak overpressure, impulse per unit area, and positive pulse duration) from the air-blast data and compared these to existing air-blast models. Peak overpressure measurements showed good agreement with the models at close ranges but tended to attenuate more rapidly at longer range (~ 1 km), which is likely caused by upward refraction of acoustic waves due to a negative vertical gradient of sound speed. We estimated yields of the MINIE2013 explosions using the Integrated Yield Determination Tool (IYDT). Errors of the estimated yields were on average within 30% of the reported yields, and there were no significant differences in the accuracy of the IYDT predictions grouped by yield. IYDT estimates tend to be lower than ground truth yields, possibly because of reduced overpressure amplitudes by upward refraction. Finally, we report preliminary results on a development of a new parameterized air-blast waveform.

Introduction

One of the most important attributes of an explosion is its yield, which quantifies the energy released in the detonation and is closely related to the damage caused by the blast. The energy released in the explosion generates mechanical motions that propagate as waves to long range (1000's of km for large explosions). Explosion yield determination has long been important to nuclear explosion monitoring for treaty verification (e.g., Werth, 1963; Romney, 2009) and also is tied to recent work on nuclear forensics (Stone, 2016). This report investigates air-blast signals from near-surface explosions for the purposes of better characterizing explosion yield.

Explosions near the Earth's surface generate waves that couple into the atmosphere and travel as air-blast, acoustic and infrasound waves, as well as into the ground as seismic waves. The amplitudes of these waves are proportional to the explosive yield, but also depend on the coupling of energy into each medium: air or solid earth. The dominant factor controlling this coupling is the scaled height-of-burst (HOB) or depth-of-burial (DOB). The partitioning of energy into air-blast and seismic waves has been quantified with data from the Humble Redwood series of explosion tests, conducted by the Defense Treat Reduction Agency (DTRA) and the National Nuclear Security Administration (NNSA) and reported by Ford et al. (2014). More recent experiments have shown the importance of material strength on the seismic coupling, but air-blast amplitudes are relatively insensitive to geologic material (Bonner et al., 2013; Rodgers et al., 2016).

The MINIE2013 experiment was a campaign of low-yield chemical high explosions conducted by Los Alamos National Laboratory (LANL). This experiment provides excellent data for nuclear forensics studies because it featured near-surface explosions and recordings of speed-of-sound (SOS) data. Specifically, the MINIE2013 series included atmospheric overpressure and seismic ground motion recordings. The explosions were conducted at emplacements from 1 m depth-of-burial (DOB, corresponding to -1 m height-of-burst, HOB) to +4 m HOB. Speed-of-sound (SOS) data were recorded at distances from 230 m to 28.5 km. Investigations of the air-blast behavior from these explosions has been reported in conference presentations by Morton and Arrowsmith (2013ab), Marcillo et al. (2014) and Morton et al. (2014). Additionally, these

data were used in a study of the acoustic coda to infer temperature changes (Marcillo et al., 2014) and a study of event detection (Carmichael et al., 2016).

Data were provided to us by LANL for the purposes of explosion air-blast characterization. We analyzed the data in several ways. Firstly, we measured canonical air-blast features and compared these with existing models. Secondly, we estimated the yields using LLNL's Integrated Yield Determination tool (IYDT). Lastly we performed some preliminary investigation of air-blast waveform fitting to develop a new parameterized air-blast waveform. This report begins by describing the data used, followed by sections on the air-blast measurements and IYDT analysis. Finally, we present a new method for fitting the observed air-blast waveforms to a parameterized wavelet. We conclude by summarizing and discussing the results and considering possible future work.

Data

The MINIE2013 experiment included nearly 70 chemical high-explosives tests ranging in masses of Composition B (Comp B) explosives from 1.7 to 14.9 kg. Assuming a relative effectiveness factor of 1.33 for the Comp B to Trinitrotoluene (TNT) equivalency, the MINIE2013 yields correspond to 2.3 kg to 19.8 kg TNT equivalent. Emplacement positions ranged from 1 m below ground surface (-1 m HOB) to +4 m HOB. The experiment also considered different charge shapes (cylinders and spheres). Figure 1 shows the range of yields and HOB's from the MINIE2013 experiment.

Data were provided in the form of continuous waveforms for overpressure and seismic sensors. In the following we only considered the overpressure (air-blast and acoustic) data. We found the seismic data to have very low signal-to-noise for the P-waves which we currently use in the IYDT. The largest signals on the seismic records appeared to be coincident with the air-blast and thus are not diagnostic of the direct seismic energy excited by the explosions. Future IYDT work will incorporate peak ground velocity measurements, but for this report, we did not use seismic data.

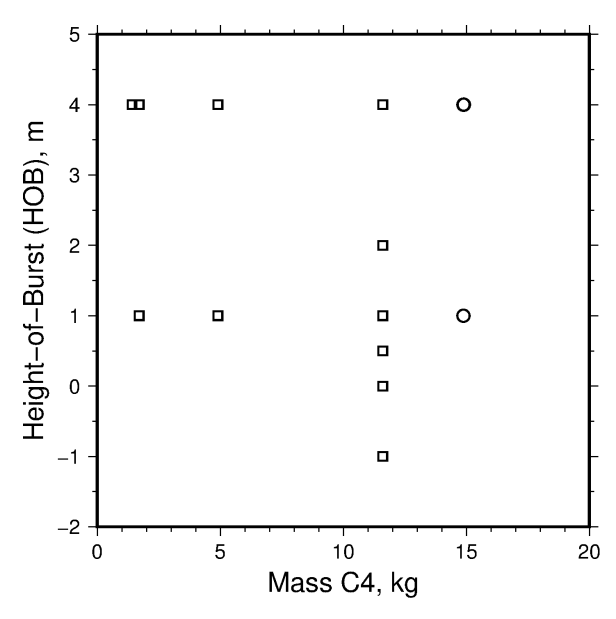


Figure 1. Masses and height-of-bursts (HOB's) from the MINIE2013 experiment. Cylinders and spheres are shown as squares and circles, respectively.

The experimental configuration is shown in the map shown in Figure 2. All explosions were located at the same source ground zero (GZ). We used data from 14 overpressure stations spanning distances from 230 m to 28.5 km. Not all stations are shown in Figure 2, but just the closest stations.

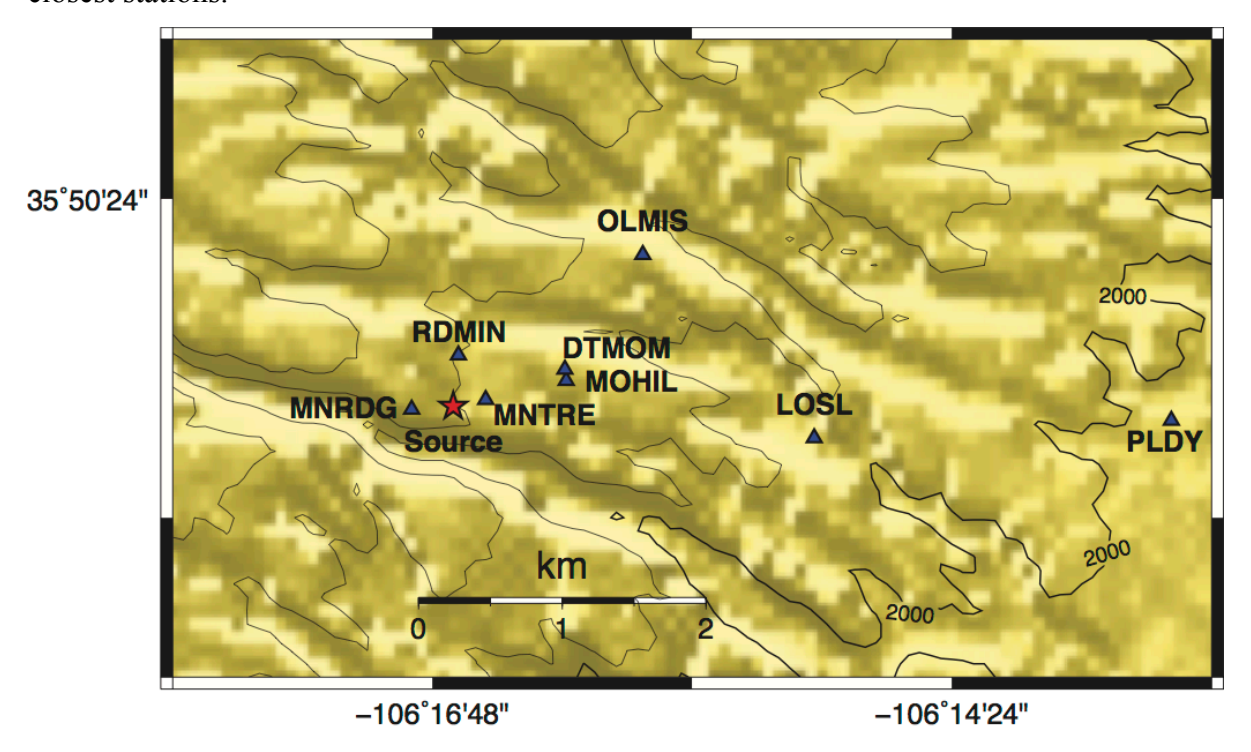


Figure 2. Map of the MINIE2013 experimental configuration showing the explosion ground zero (star, the same for all shots) and the overpressure station locations (triangles) considered herein.

Air-Blast Measurements

We measured canonical air-blast features in order to quantify air-blast behavior and compare these with reported models. We measured the peak overpressure, impulse of the positive phase, positive pulse duration and arrival velocity (distance divided by travel time). These measurements are compared to the classical air-blast model (hereafter called KG85) reported by Kinney and Graham (1985). In addition we compare the impulse measurements with two models used in the IYDT: Ford et al. (2014) and the more recently developed model IYDT 2016.

Air-blast features were measured automatically first by determining a 15 s window using the known distance and estimated arrival time based on the speed of sound in a standard atmosphere. The peak pressure in this window was used to define the air-blast arrival time. We then defined the beginning and end of the air-blast positive phase by the zero crossings surrounding this peak and the duration was taken as this time interval. We used several criteria to eliminate ambiguous peaks within these windows. Measurements were only made on the waveform if the timing of the arrival was less than 3.0 seconds away from the expected values (based on the typical speed of sound, 343 m/s), the peak overpressure in the window was required to be at least .02 Pa, and we required one candidate air blast peak in the window.

Air-blast features were compared to reported models. In order to compare features from explosions of differing yields, we used hydrodynamic scaling and plotted the scaled features versus scaled range along with the model predictions. Figures 3-5 show the peak overpressure, scaled impulse and scaled duration versus scaled range for the MINIE2013 data set.

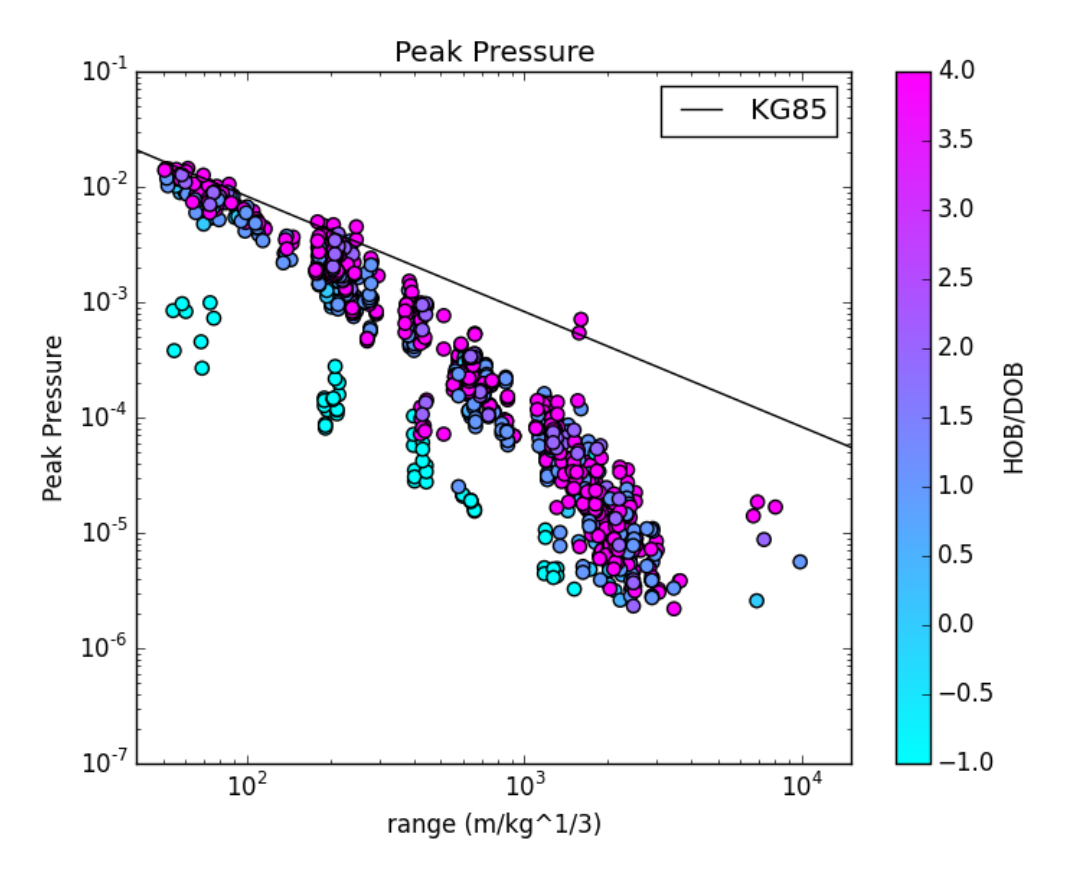


Figure 3. Peak overpressure vs. scaled range measured on the MINIE2013 data and compared to KG85 peak overpressure model for HOB=0.

The peak overpressure (Figure 3) and impulse (Figure 4) measurements are consistent with the KG85 models out to about 200-500 m range but begin to diverge from the models at long range due to propagation effects. The impulse measurements tend to be less scattered and are closer to the model predictions than the peak overpressure measurements. For these plots the yield was derived from the TNT equivalent and measurements were adjusted for the ambient atmospheric temperature and pressure (~80,000 Pa). We also accounted for the surface emplacement in a half-space by doubling the yield.

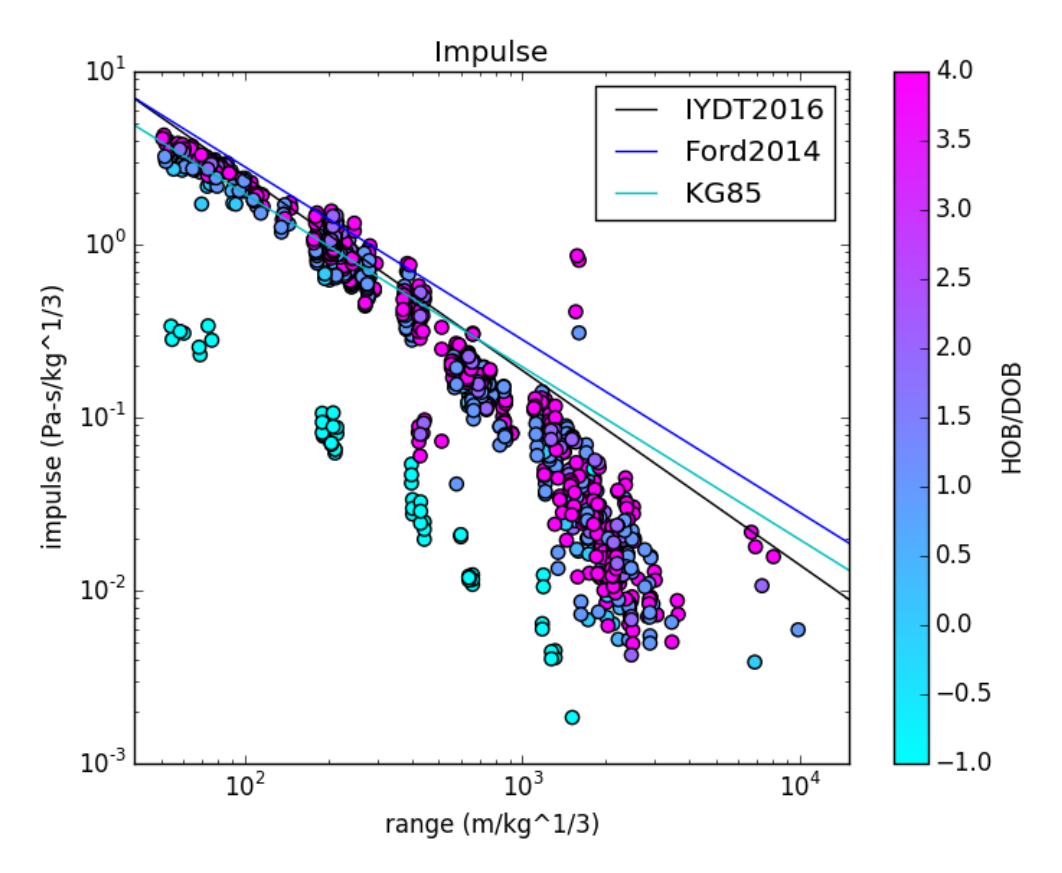


Figure 4. Scaled impulse vs. scaled range measured on the MINIE2013 data and compared to KG85, Ford2014 and IYDT 2016 models for HOB=0.

The measured positive pulse durations are shown in Figure 5. These data are not consistent with the KG85 model: the data display a trend with range and are shifted higher than the KG85 prediction. A very similar behavior of air-blast positive phase duration with range was reported by Koper et al. (2002). The consistency of our impulse and peak overpressure measurements with KG85 and other impulse models suggest that this discrepancy in duration is not due to a problem with our measurement method. It is possible that the KG85 positive phase duration model is biased.

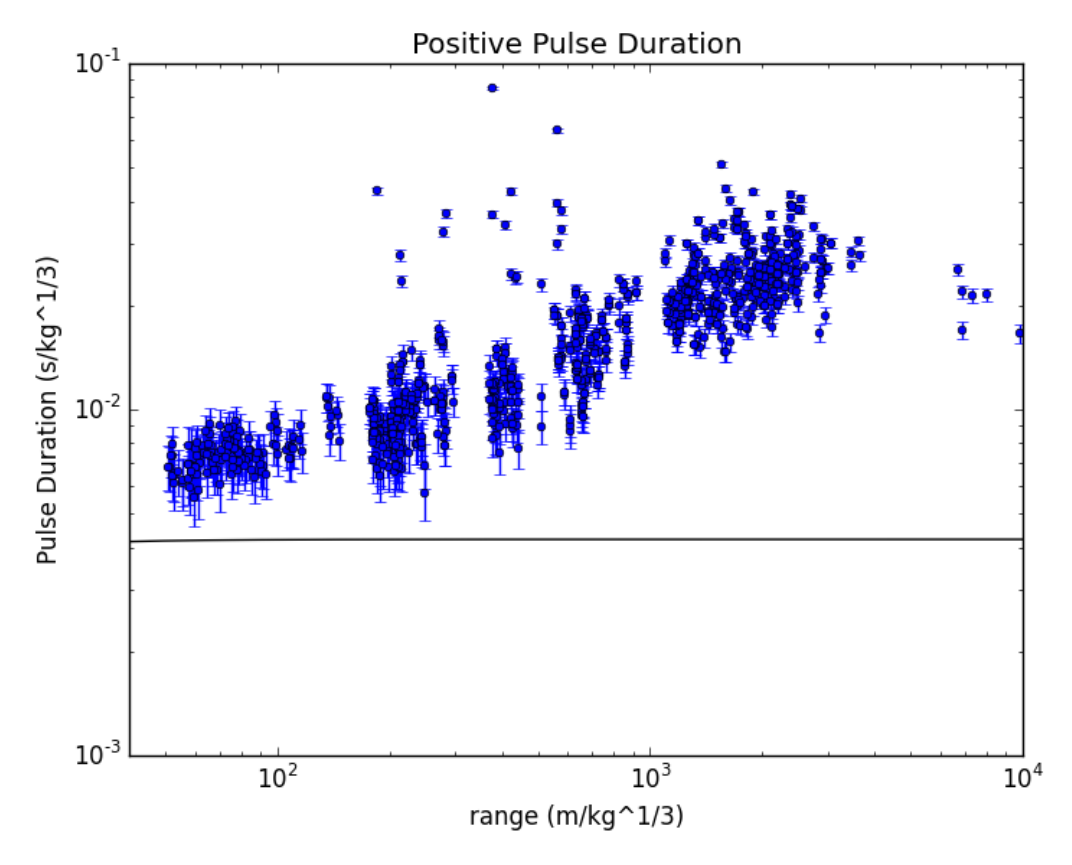


Figure 5. Positive pulse duration vs. scaled range measured on the MINIE2013 data and compared to KG85 model. Error bars are taken as the sample rate.

We also measured the travel velocity of the air blasts. We divided the distance, computed from the reported latitudes and longitudes of the explosions and stations, by measured travel time. We measured the travel time by taking the difference between the reported detonation time and the zero crossing recorded during the blast waveform detection process described previously, which measures the onset of the air-blast. Figures 6 and 7 show the measured air-blast arrival velocity as a function of scaled range with color-coding by HOB and yield, respectively.

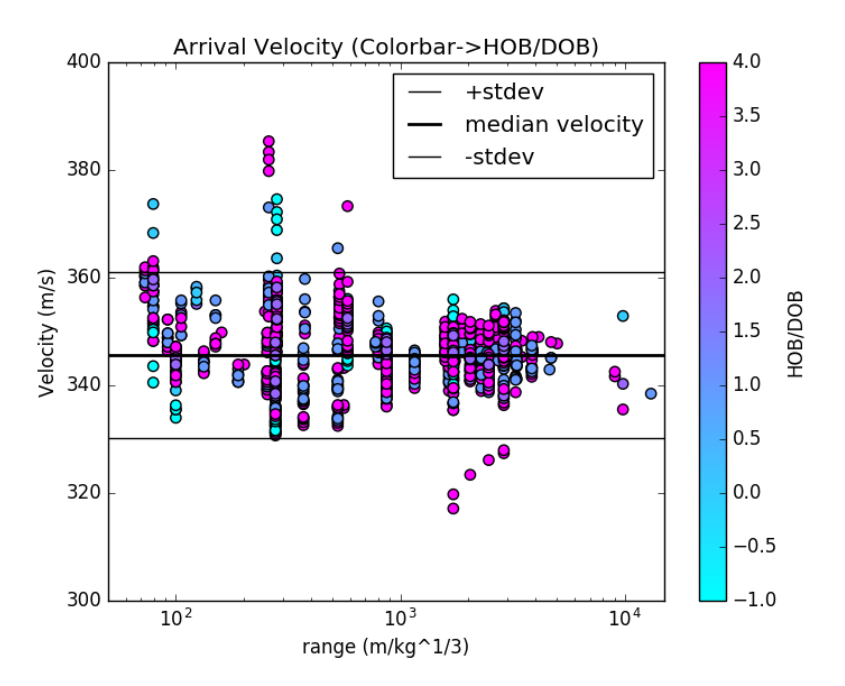


Figure 6. Velocity of the air blast computed by dividing the source-station distance by the measured travel time.

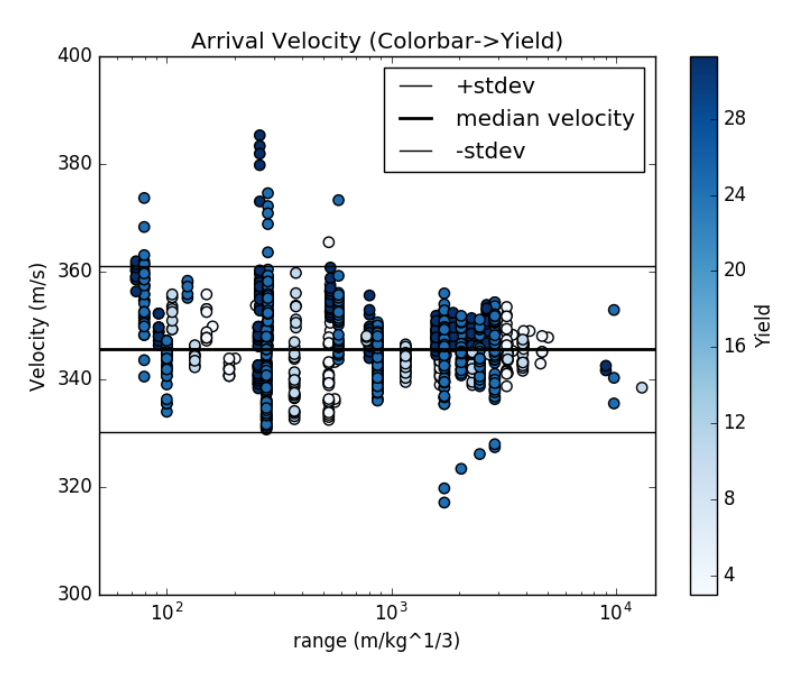


Figure 7. Velocity of the air blast computed by dividing the source-station distance by the measured travel time.

The travel times are consistent with the expected speed of sound (343 m/s), suggesting that our method of detecting the blast arrival is sufficiently accurate. No clear trend of the arrival velocities with HOB and yield can be seen. In fact these variations in arrival velocity are likely due to variations in sound speed related to temperature (Marcillo et al., 2016). Further investigation could be done if we are able to access in situ temperature measurements.

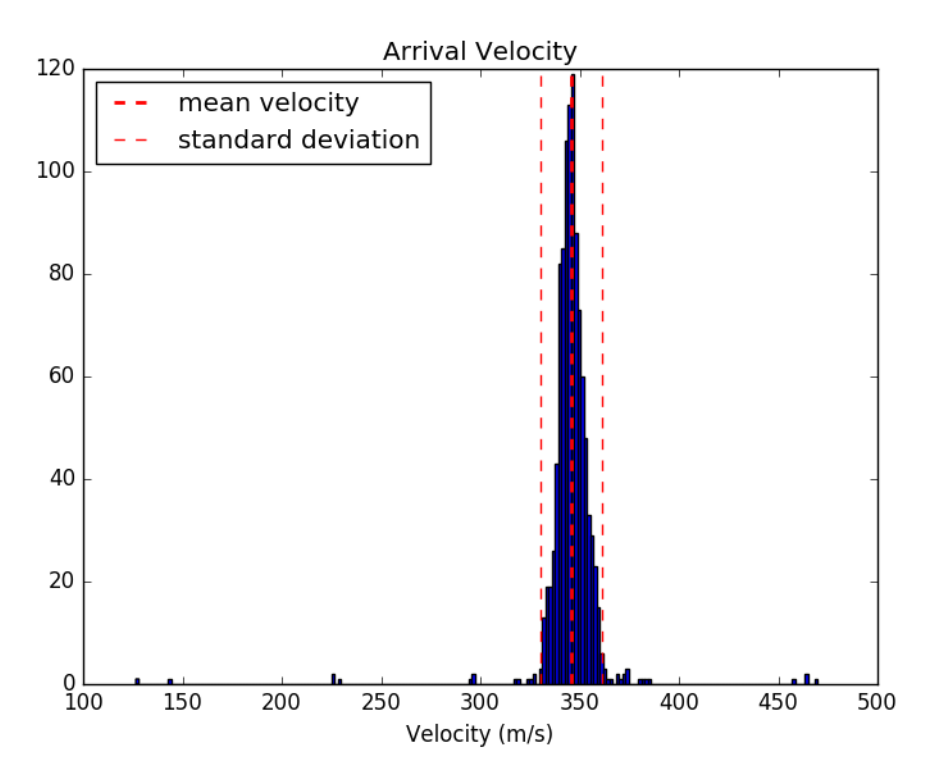


Figure 8. Histogram showing the travel velocity of the air blast arrival.

Figure 8 shows a histogram of the arrival velocities from all air-blast waveforms that provided acceptable measurements. The data are strongly distributed around the average speed-of-sound in air (Figure 8).

The impulse measurements shown in Figure 4 show a very linear trend on the log base-10 scaled impulse versus log base-10 scaled range at short ranges (<500 m/kg^{1/3}) and follow the reported models with approximately 1/R spherical spreading. However, at longer range the impulse amplitudes decay more rapidly than 1/R. We have seen this behavior in other data sets and shown with full waveform modeling that this can be reproduced by reduction of sound speed with altitude (negative sound speed gradient). This topic is the subject of further work.

LLNL's IYDT software uses a large suite of models relating the measured impulse to yield, range and HOB. One such model, IYDT2016, gives the minimum misfit between data and predictions. We demonstrate that by introducing a nonlinear (in log space) term to the IYDT2016 scaled impulse vs. scaled range model it is possible to capture the nonlinearity of the data. The following non-linear model was fit to the scaled impulse data using a least-squares method for the above ground MINIE shots:

$$log_{10}(Impulse) = a + b * log_{10}(rs) + d * hs$$

$$log_{10}(Impulse) += c * log_{10} \left(\frac{1}{rs^2}\right) * log_{10}(rs)$$

$$log_{10}(Impulse) -= log_{10} (1 + 10^{(d*10*hs)})/10$$

 $Impulse = 10^{log_{10}(Impulse)}$

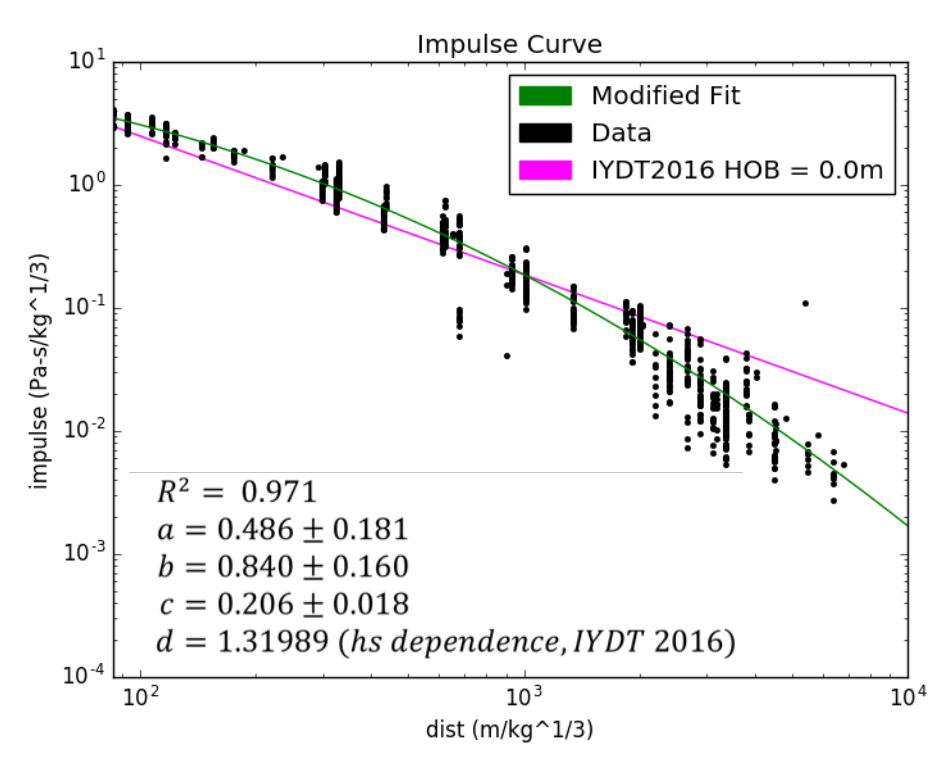


Figure 9. Scaled impulse measurements (dots) versus scaled range with the IYDT 2016 model (magenta) and the modified model (green).

Figure 9 shows the impulse values along with the IYDT2016 (linear) and modified (non-linear) models. One can see that at close range the IYDT2016 model predicts the observed MINIE2013

impulse values quite well, however the fit degrades with range. The modified model includes curvature, which fits the amplitudes at longer range better than the IYDT 2016 model. In future work we seek to develop a parameterized impulse vs. range model that takes into account propagation effects and accurately predicts how the impulse behave nonlinearly. Using such models we could potentially extend the range over which IYDT is effective.

Integrated Yield Determination Tool (IYDT) Analysis of MINIE2013 Data

The Integrated Yield Determination Tool (IYDT) estimates explosion yield (W) and height-ofburst (HOB) from air-blast overpressure and seismic ground motion time-series. It uses models for the air-blast impulse and seismic P-wave zero-to-peak displacement as these were found to provide robust estimates of yield (Koper et al., 2002; Ford et al., 2014). The IYDT uses models of SOS signal behavior calibrated from numerous explosion experiments. These explosions do not include MINIE2013 and in fact had much larger yields (200-50,000 kg TnT equivalent). The IYDT uses a range of models derived from a stochastic process using a Markov Chain Monte Carlo (MCMC). The variation in the signal models and the estimated error between data and prediction communicate the model uncertainty and this is mapped into yield uncertainty by the IYDT. The IYDT uses two methods to estimate W and HOB: grid search and MCMC. Both methods use Bayesian approaches. In each method the likelihood function is formed using a suite of stochastic signal models from the above-mentioned MCMC process. The range of these models reflect the uncertainty in signal excitation and propagation as seen by the calibration data. In fact the models include a variance of the calibration data about each model. This variance is used in the denominator of likelihood function. The grid search involves a straightforward search over the W-HOB model space with a uniform grid (logarithmic base-10 W – linear HOB), however the likelihood at each W-HOB pair is based on a suite of stochastic signal models. We typically used 1000 models per W-HOB point considered in the grid search. The MCMC yield estimation process uses a user-specified number of chains and searches the W-HOB model space with a random walk, guided by acceptance/rejection criteria based on the Metropolis-Hastings algorithm (Hastings, 1970). The MCMC algorithm is able to better map the fine structure of the high-likelihood region of the W-HOB model space and it is used to report confidence intervals (typically 5% and 95%). We typically used 4 MCMC chains with 100,000 iterations per chain in the MCMC inversions in this report.

The IYDT uses the different sensitivity of overpressure and seismic signals to HOB to break the trade-off between W and HOB. Because of extremely low P-wave signal-to-noise we did use the seismic data in the MINIE2013 experiment we only considered the air-blast data from the MINIE2013 series. Consequently, we have difficulty breaking the trade-off between yield and HOB. To mitigate this problem we limited the HOB search range to the near-surface or above ground. For the majority above ground shots we used 0 to 5m and for below ground shots we used the range from -3 to 1 m. It was necessary to use a search region that includes positive values for the buried shots in order for the MCMC inversion to converge. Despite this, both of the inversion methods were successful in predicting the correct HOB for below ground shots. For air-blast impulse, the IYDT models show very little variation with HOB for the above ground yield range we used. This tends to cause the inversions to collapse to the same HOB value (0m for Grid Search and ~2.5m for MCMC) for all above ground shots.

IYDT Event Results

The following is an example of a typical analysis of an event using the IYDT. This event had a yield of 15.4 kg TNT equivalent and a height of burst of 2m. Because no seismic data was useable, the result for the height-of-burst/depth-of-burial prediction is not expected to be accurate. As this was an above ground event, the height-of-burst search range was defined to be 0 to 5m. One air-blast measurement with an unusually large uncertainty has been excluded from both the grid search and MCMC inversions (see large error bar in Figure 10). Note that the data point excluded was low amplitude and long range, most likely impacted by propagation effects. We note that the IYDT software had to be modified when applied to the MINIE2013 data to search for much lower yields than have typically been considered.

Figure 10 shows the grid search results. The left panel shows the likelihood in the W versus HOB space. Warm colors indicate high likelihood and the results show that W is well determined. Conversely, HOB is not well resolved and the likelihood shows nearly uniform estimates of he HOB across the range. The right panel shows the impulse predictions from the highest likelihood model versus the measured air-blast impulse values. The error bars shown on individual measurements were derived from the IYDT's signal processing algorithm. Ideally

these points should lie on the 1-to-1 line plotted in the panel. Measurements are color-codes by azimuth. No seismic were used and consequently, no data are shown in the lower right (seismic) panel.

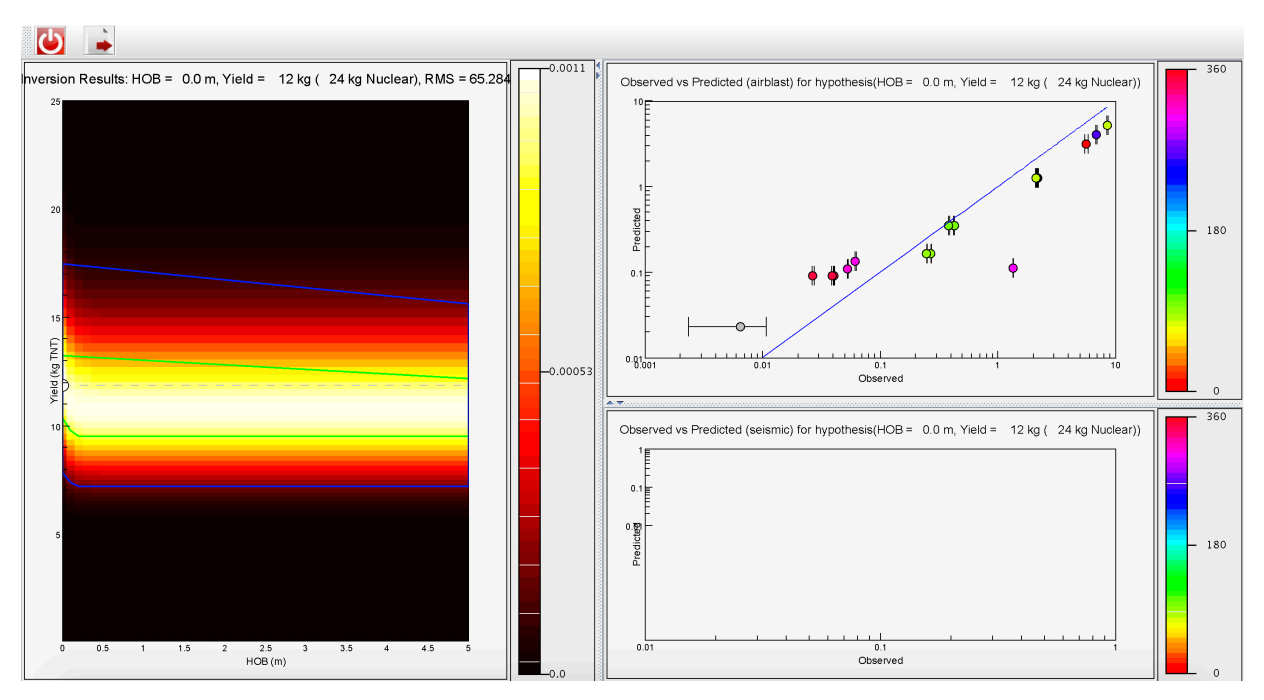


Figure 10. The results of the grid search inversion method for the 15.4 kg event. The maximum likelihood model prediction for yield was 12kg. There was no useable seismic data available for this event.

The MCMC results are shown in Figure 11. The panel on the left reports the summary results in text form. The panel on the right shows a histogram of the accepted yield values. This is unimodal, but not symmetric. In the left panel, we report the median, mean, standard deviation and the 5% and 95% intervals (red vertical lines in histogram plot). To standardize reporting of preferred values we typically use the median yield value and 5% and 95% intervals as uncertainties. Thus for this explosion we estimate the yield to be 12 kg with range 9-16 kg. The ground truth yield value is 15.4 kg. Note that currently we only report yield values to the nearest kilogram because we have never before worked with such low yield values. We will consider changing the precision of these reports for low-yield cases.

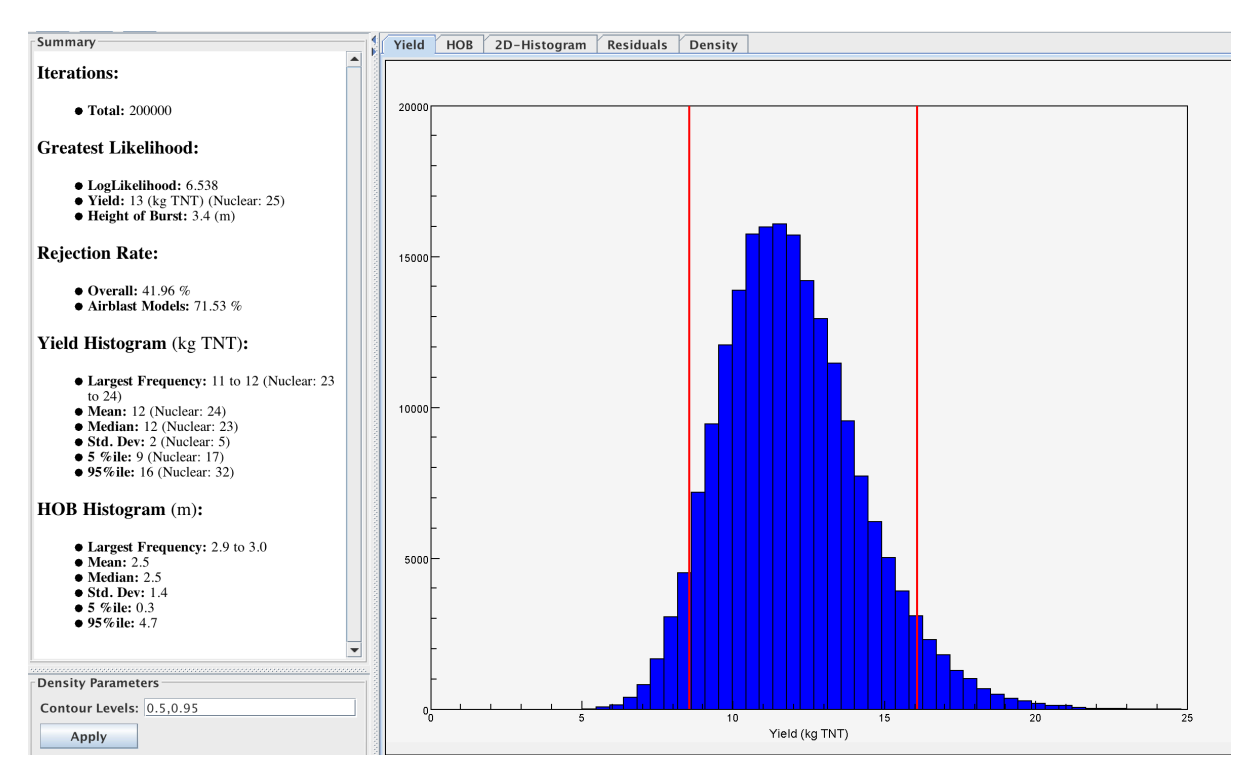


Figure 11. The results of the MCMC stochastic inversion method for a 15.4 kg explosion. The median of the models was 12 kg (consistent with the grid search method). The 5% point on the probability distribution is 9 kg and the 95% is at 16 kg (red lines).

The IYDT produces other graphical results from the MCMC inversion, but these are beyond the scope of this report.

IYDT Variance Analysis

We estimated the yield for 67 MINIE2013 explosions using the IYDT. Figure 12 shows the estimated yield and uncertainty (5% and 95% intervals) along with the ground truth yield for each shot. IYDT estimates tend to be lower than ground truth yields, possibly because of reduced overpressure amplitudes by upward refraction. Upward refraction reduces amplitudes relative to the simple models used in IYDT such as the IYDT2016 model shown Figure 9. For many of the larger shots the true yields are within the IYDT estimated uncertainty. The lower yield estimates tend to have higher confidence (lower uncertainties), but this may be due to only a few nearby stations having usable signals. Furthermore, the comparison of median yield and error bars could be impacted by low precision of the reported median and uncertainty values.

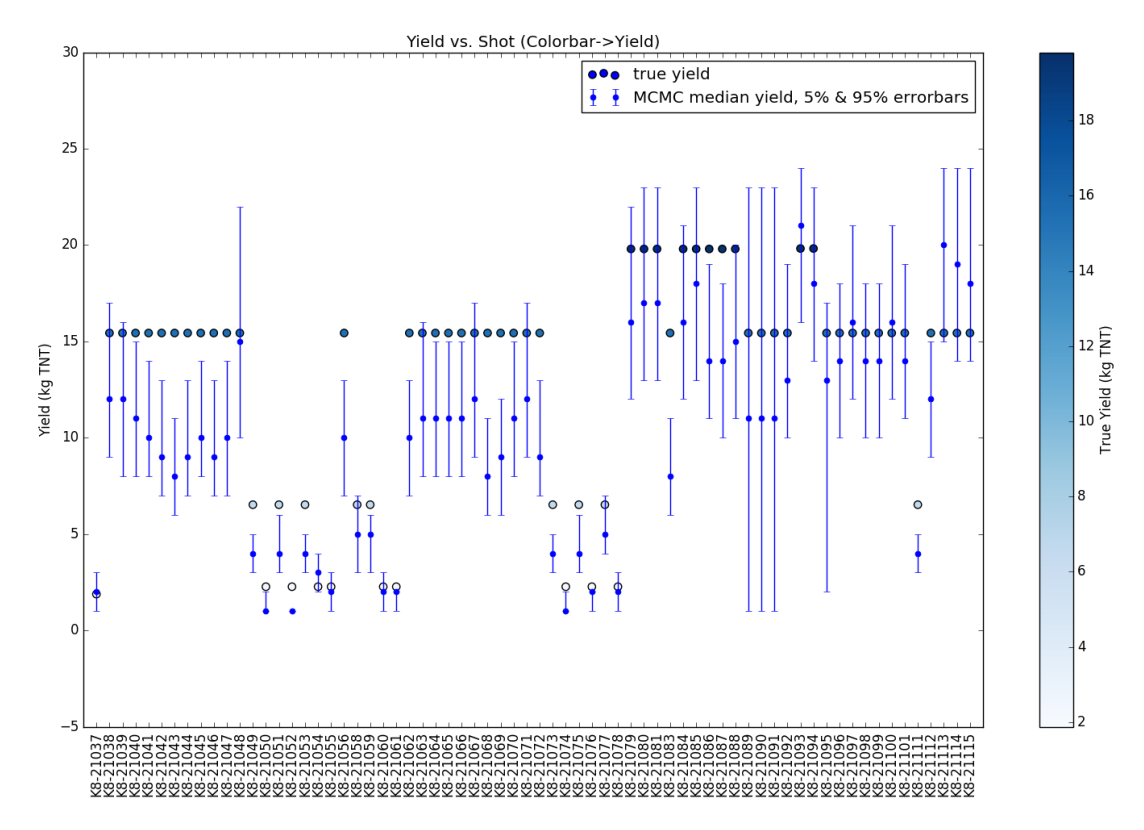


Figure 12. Estimated yield and uncertainties (blue circle with error bars) compared with ground truth yield (circles color-coded by yield) for 67 MINIE2013 explosions plotted as a function of shot name.

In order to determine the performance of the IYDT to estimate the yield of the MINIE2013 detonations, we analyzed the difference between the reported and IYDT predicted yield values. The seismic data was not useable in this data set, limiting the inversions to using only air blast data. The IYDT air-blast models are not strongly sensitive to the HOB or DOB in the ranges seen in the MINIE data. Therefore, the HOB/DOB predictions are not necessarily expected to be accurate. Interestingly, Morton et al. (2014) report a monotonic increase in impulse amplitudes with HOB. Further analysis of the MINIE2013 data and its dependence on HOB could be carried with other data sets, such as the HUMBLE REDWOOD data considered in Ford et al. (2014).

A histogram of the yield error, expressed in percent difference is shown in Figure 13. Yield errors range from less than 10% to over 50%. The largest yield errors were for the smallest yield

explosions, which could be influenced by signal-to-noise or yield reporting precision. The mean percent difference between the reported and IYDT predicted yield values is less than 30% suggesting that the models used in IYDT, which were developed for significantly higher yield detonations, are indeed applicable to small yield explosions.

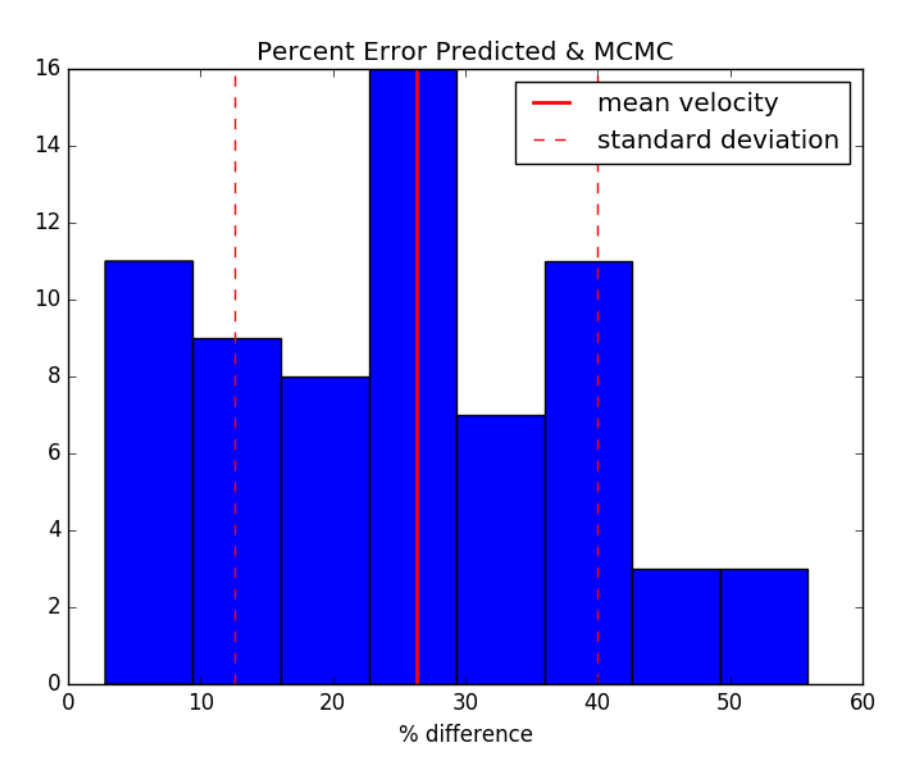


Figure 13. A histogram showing the percent difference between the expected yield and the IYDT predictions

Figure 14 shows box-and-whisker plots of the yield estimation errors in percent difference vs. actual yields of events. All events were divided into four groups based on their reported yields (2.2 - 19.8 kg TNT equivalent), and the box-and-whisker diagrams were drawn for each group. The bottom and top of each box correspond to the first and third quartiles, and the horizontal band inside the box indicates the median of each group. The whiskers extend to 1.5x interquartile range from the first quartile to third quartile. Each group shows different median and quartiles in estimation error, which might be affected by yields of explosions. We conducted an analysis of variance (ANOVA, Davis, 1986) in order to check for statistically significant differences in the errors among these groups.

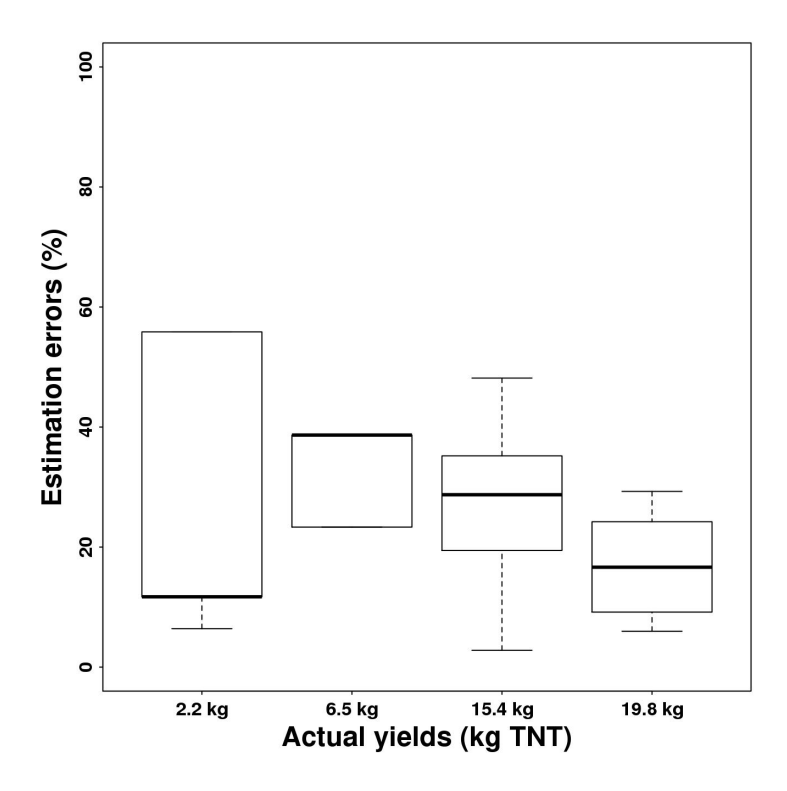


Figure 14. The box-and-whisker plot of estimation errors for above ground detonations grouped by true yield. The each box ranges from the first quartile to the third quartile, and the band inside the box indicates the median of the group. The whiskers extends to 1.5x interquartile distance.

In general, the technique of ANOVA involves separating the total variance of measurements into various sources of variance, from example, variance between groups and within groups. The equality of each group is tested by simultaneously considering both differences in means and in variances. Table 1 shows an ANOVA table for MINIE2013 measurements grouped by yields. The mean squares in the table are the sample-based estimate of variances, indicating that the observed variance between groups is larger than variance within groups. The equality of each group is determined by the F-test.

Source of variance	Sum of square	Degree of freedom	Mean square	F statistics
Between Groups	1290.581	3	430.1937	2.287
Within Groups	11285.08	60	188.0847	

Total	12575.58	63	199.6124	
-------	----------	----	----------	--

Table 1. An ANOVA table for MINIE2013 explosion measurements shown in Figure 14.

Figure 15 shows probability distribution of F statistics shown in Table 1. If the means of each group are the same, 95% of randomly drawn events will fall into the area below F=2.758, and only 5% of events will have larger F values. The computed F value in Table 1 falls out of the 5% critical region, and we can conclude that the mean values of those groups are not statistically different at the level of 5% significance.

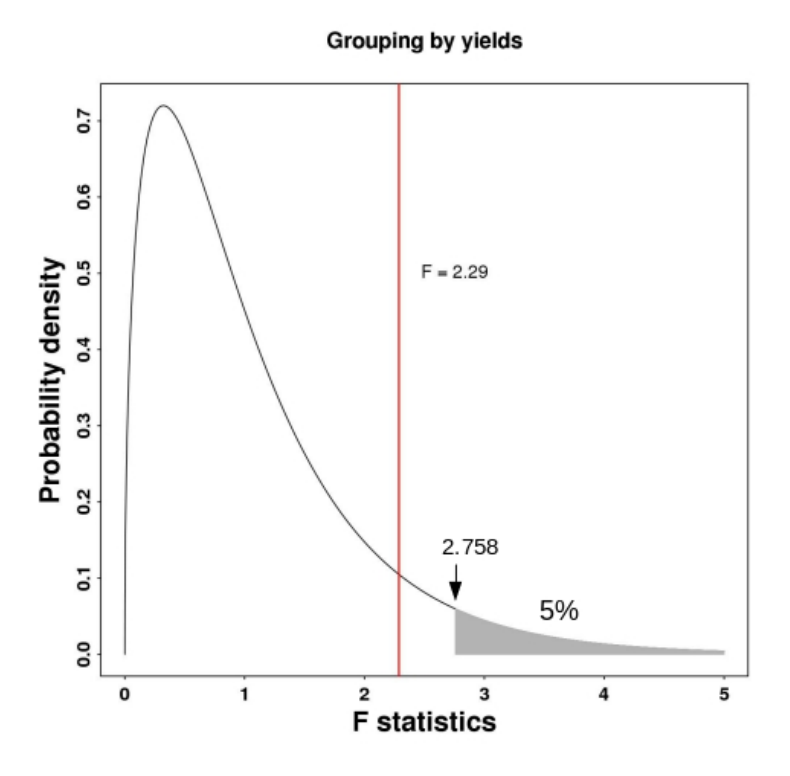


Figure 15. Results of the ANOVA analysis in Table 1. The F value of the analysis falls into 95% probability region below F=2.758, leading the conclusion that means of those groups are not significantly different at 5% significance.

The result of the ANOVA analysis shows that there is not a significant difference among the percent error due to yield. This is encouraging as it confirms that, in terms of percent error, the IYDT predictions are not significantly different for all explosion yields in the MINIE2013 detonations, which ranged from 2 to 20 kg TNT equivalent. Not only are the IYDT predictions reasonably accurate at small yields the measurement accuracy also does not diminish as

detonation yield is decreased. Note however, that the median yield decreases with yield. Our estimates of yield error may be compounded by weaker signals (lower signal-to-noise) and the low precision of yield reports.

Waveform Fitting to Derive a New Parameterized Air-Blast Model

Air-blast waveforms have been parameterized using models that can generate the time-history of overpressure for a range of yields and distances. The classical Kinney and Graham (1985, hereafter referred to as KG85) air-blast models are widely used in explosion air-blast studies. These rely on hydrodynamic scaling and tabulated parameters for chemical and nuclear explosions. While the KG85 provides a model for wide application, it has several shortcomings; the main being that the parameterized overpressure time-history has an instantaneous infinite increase in overpressure at the time of the blast arrival. Also the KG85 model is only truly applicable to the hydrodynamic region for a homogeneous atmosphere, consequently it does not include the commonly observed reduction of the air-blast rise time with range as the air-blast energy dissipates and/or interacts with sound speed gradients. We have shown evidence that KG85 does not match the positive phase duration for above ground explosions, consistent with Koper et al. (2002). Finally, the KG85 waveform typically does not accurately represent the negative phase of observations.

The acoustic waveform inversion method of Kim and Rodgers (2016) estimates the pressure time-history of the equivalent acoustic source and then relies on KG85 scaling relationships to estimate the explosion yield. We have used finite difference time domain (FDTD) modeling but would require very dense meshing to capture high-frequency energy associated with rapid blast-wave onset. Thus it is desirable to have a new parameterized air-blast waveform model that can be used for yield estimation and FDTD simulation with band limited signals and realistic propagation effects.

We have begun investigations that seek to develop a new air-blast waveform for the purposes of yield estimation and simulation. These models are based on the functional forms of derivatives of the stable distribution, which is a generalization of the Gaussian distribution. The first derivative of the approximate Landau distribution (Figure 16), a special case of the stable

distribution, is successfully fit to MINIE2013 air-blast data using an iterative least-squares method using initial guesses based canonical air-blast measurements. We use the derivative of the Moyal approximation (Moyal, 1955) of the Landau distribution:

Landau PDF Approximation =
$$\frac{1}{\sqrt{2\pi}}e^{-\frac{1}{2}(x+e^{-x})}$$
$$\frac{d}{dx}\left(Landau PDF\right) = \frac{1}{2\sqrt{2\pi}}e^{-\frac{1}{2}(3x+e^{-x})}(1-e^x)$$

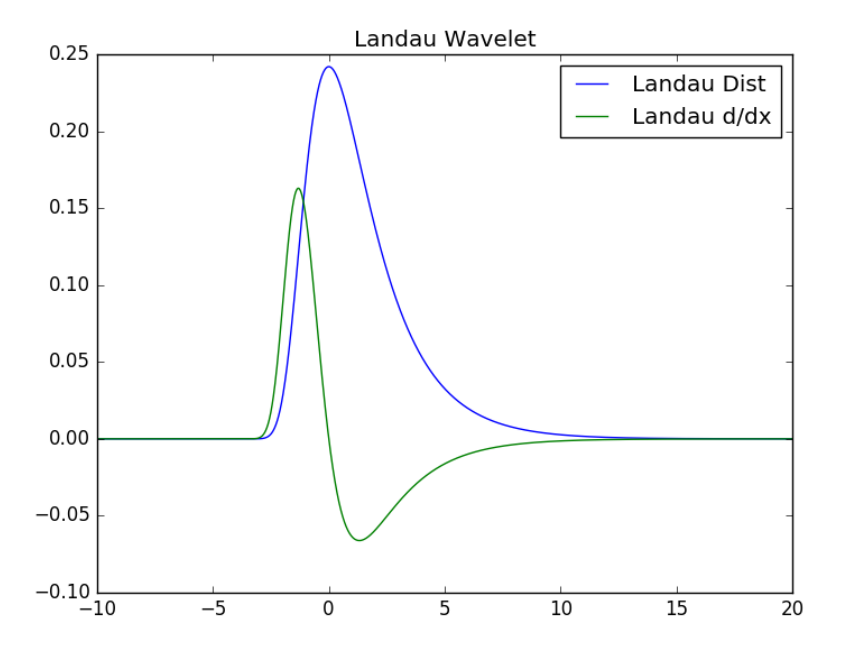


Figure 16. The approximation of the Landau distribution (blue) and its first derivative (green).

The Landau derivative function is a true wavelet in that is begins at zero, oscillates, and then decreases back to zero. It is also impulse balanced as the positive and negative area under the curve sums to zero. We fit the Landau derivative wavelet to the MINIE2013 air-blast data by adjusting the scaling of the wavelet:

$$Pressure = \frac{h}{2} * e^{-\frac{1}{2} \left(\frac{3(x-p)}{c} + e^{-\frac{x-p}{c}} \right)} (1 - e^{\frac{(x-p)}{c}})$$

$$Impulse = h * e^{-\frac{1}{2} \left(\frac{(x-p)}{c} + e^{-\frac{(x-p)}{c}} \right)}$$

h, c, p control position and scaling p is fixed to the zero crossing

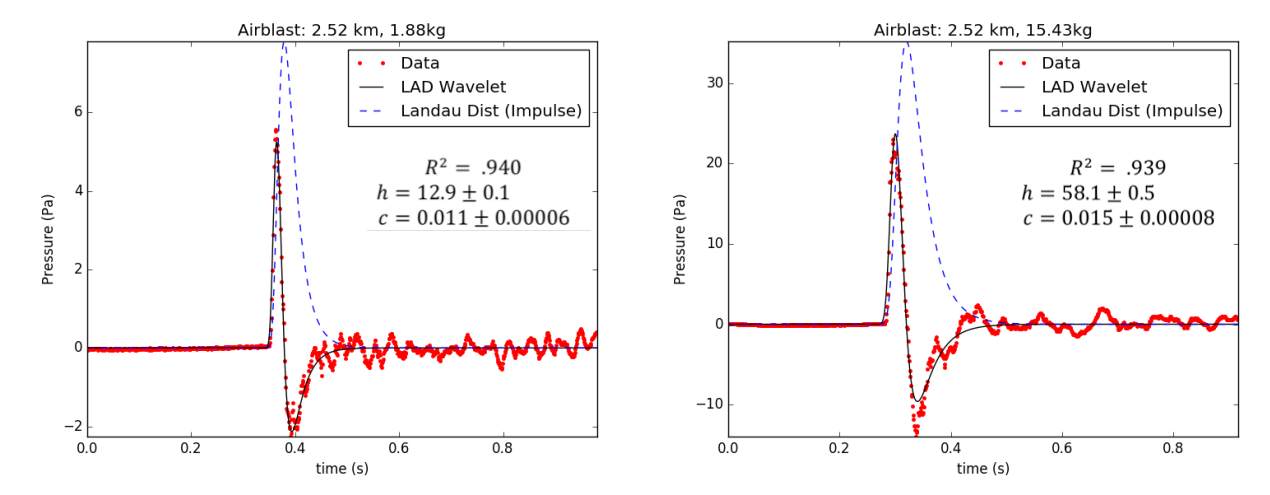


Figure 17. Example fits of MINIE2013 air-blast data (red) to the Landau derivative wavelet (black). The blue dashed line shows the integral of the Landau derivative wavelet and corresponds to the impulse measurement.

Preliminary fitting results (Figure 17) are encouraging – the first derivative of the Landau function fits the air-blast data very well. However, it is clear that we will need to generalize the model by introducing an additional fitting parameters that control the yield-dependent shape of the wavelet in order to accurately fit all air blasts. Once such the scaling relationships are developed, we will investigate the ability of the new model to accurately and consistently reproduce canonical air-blast parameters. We can then begin to look for direct relationships between the parameters of the new air-blast model and yield.

Discussion, Conclusions and Future Work

The MINIE2013 air-blast data are valuable for testing signal models and yield estimation algorithms for above ground explosions. We have analyzed these data and show that canonical air-blast features are consistent with expected values. The decay of amplitudes with range is more rapid than expected from models based on a homogeneous atmosphere, as we have observed before. This topic warrants further investigation, especially when in situ atmospheric conditions are available (e.g. altitude-dependent temperature and wind profiles). Additional analysis of the raw measurements could constrain estimates of the variability in path propagation effects for air-blast and will be the subject of further investigations.

Estimates of yield using the Integrated Yield Determination Tool (IYDT) from air-blast only are quite good, with mean yield error less than 30% and on the same order as the calibration data used to derive signal models. This is remarkable because the IYDT's signal models were derived from much larger yield explosions (by 20-1000 times). This is very encouraging for applying the IYDT to low yield events. Analysis of variance indicates that the yield error is consistent across the yield range.

Preliminary investigations of fitting a new functional form to air-blast waveforms shows great promise. The first derivative of the Landau function shows strong similarity to air-blast waveforms. We will be pursuing the development of this new parameterized air-blast waveform to improve deficiencies of the classical Kinney and Graham (1985) air-blast waveform. This will have application in waveform-based yield estimates following Kim and Rodgers (2016).

Acknowledgements

We are grateful to Richard Stead and Omar Marcillo, both of Los Alamos National Laboratory. RS provided the MINIE2013 waveforms and metadata and crucial assistance. OM provided valuable assistance with the overpressure instrument responses that helped us verify the amplitudes. We thank OM and Emily Morton for copies of their conference presentations.

Support for this work was provided by the National Nuclear Security Agency, Nuclear Forensics Program, F-2016 Venture. This work was performed under the auspices of the U.S. Department of Energy by Lawrence Livermore National Laboratory under contract DE-AC52-07NA27344.

References

Bonner, J. L., D. R. Russell, and R. E. Reinke (2013), Modeling surface waves from aboveground and underground explosions in alluvium and limestone, Bull. *Seismol. Soc. Am.*, 103, 2953–2970, doi:10.1785/0120130069.

Carmichael, J. D., R. Nemzek, S. Arrowsmith and K. Sentz (2016). Fusing geophysical signatures of locally recorded surface explosions to improve blast detection, *Geophys. J. Int.*, 204, 1838–1842,

Davis, J. C., (1986). Statistics and Data Analysis in Geology, Second Ed., Wiley, New York, 646 pp.

Ford, S. R., A. J. Rodgers, H. Xu, D. C. Templeton, P. Harben, W. Foxall, and R. E. Reinke (2014), Partitioning of seismoacoustic energy and estimation of yield and height-of-burst/depth-of-burial for near-surface explosions, *Bull. Seismol. Soc. Am.*, 104, 608–623, doi:10.1785/0120130130.

Gitterman, Y., and R. Hofstetter (2014), GT0 explosion sources for IMS infrasound calibration: Charge design and yield estimation from near-source observations, *Pure Appl. Geophys.*, 171(3–5), 599–619, doi:10.1007/s00024-012-0575-4.

Hastings, W.K. (1970). Monte Carlo Sampling Methods Using Markov Chains and Their Applications, Biometrika. 57 (1): 97–109. doi:10.1093/biomet/57.1.97.

Kim, K., D. Fee, A. Yokoo, and J. M. Lees (2015), Acoustic source inversion to estimate volume flux from volcanic explosions, *Geophys. Res. Lett.*, 42, 5243–5249, doi:10.1002/2015GL064466.

Kim, K., and A. Rodgers (2016), Waveform inversion of acoustic waves for explosion yield estimation, *Geophys. Res. Lett.*,43, doi:10.1002/2016GL069624.

Kinney, G., and K. Graham (1985), Explosive Shocks in Air, 282 pp., Springer, Berlin and New York.

Koper, K. D., T. C. Wallace, R. E. Reinke, and J. A. Leverette (2002), Empirical scaling laws for truck bomb explosions based on seismic and acoustic data, Bull. Seismol. Soc. Am., 92(2), 527–542, doi:10.1785/0120000242.

Marcillo, O., S. Arrowsmith, R. Whitaker, E. Morton, and W. Scott Phillips (2016). Extracting changes in air temperature using acoustic coda phase delays, *J. Acoust. Soc. Am.* 136

Marcillo, O., S. Arrowsmith, and E. Morton (2014). Acoustic Signatures of Different Explosive-Detonator Configurations in Small HE Explosions (abstract, poster), presentation at the Seismological Society of America, Apr. 2014, LA-UR-14-22757.

Morton, E.A., Arrowsmith, S.J., Marcillo, O., Whitaker, R. (2014). An Analysis of Repeating Explosions Using Seismoacoustic Data (abstract, poster), presentation at the Seismological Society of America, Apr. 2014

Morton, E.A., Arrowsmith, S.J. (2013). An Empirical Study of Acoustic/Infrasonic Source and Propagation Effects Using a Large Dataset of Explosions (abstract, slides), presentation at the Acoustical Society of America, Dec. 2013, LA-UR-13-28912.

Morton, E.A., Arrowsmith, S.J. (2013). An Empirical Study of Acoustic/Infrasonic Source and Propagation Effects Using a Large Dataset of Explosions (abstract, poster), presentation at the American Geophysical Union, Dec. 2013, LA-UR-13-28986

Moyal J. E. (1955). Theory of ionization fluctuations, The London, Edinburgh, and Dublin Philosophical Magazine And Journal Of Science, 46, 374.

Romeny, C. (2009). Detecting the Bomb: The Role of Seismology in the Cold War, New Academia Publishing, 324 pages.

Stone, R. (2016). Who dropped the bomb? Postdetonation forensics may help provide answers if the nuclear nightmare becomes a reality, *Science*, 351, 627811, March 2016.

Werth, G. C., and R. F. Herbst (1963), Comparison of amplitudes of seismic waves from nuclear explosions in four mediums, *J. Geophys. Res.*, 68(5), 1463–1475, doi:10.1029/JZ068i005p01463.